Dalton Transactions

Accepted Manuscript

ROYAL SOCIETY OF CHEMISTRY

www.rsc.org/dalton

Journal Name

ARTICLE

Neutral, heteroleptic copper(I)-4*H*-imidazolate complexes: synthesis and characterization of their structural, spectral and redox properties†

Received 00th January 20xx,
Accepted 00th January 20xx

DOI: 10.1039/x0xx00000x

www.rsc.org/

M. Schulz,*[a,b] F. Dröge,[a] F. Herrmann-Westendorf,[a] J. Schindler,[a,b] H. Görls[c] and M. Presselt [a]

Facile synthetic access to four novel, neutral, heteroleptic copper(I)-complexes, incorporating 4*H*-imidazolates as well as the bisphosphane ligands XantPhos and DPEPhos is reported. The complexes were characterized in the solid state as well as in solution by means of single crystal X-ray diffraction as well as NMR spectroscopy, mass spectrometry and elemental analysis. The copper(I)-4*H*-imidazolate complexes show a broad intense absorption that spans almost the entire visible range. TD-DFT calculations revealed the charge transfer character of the underlying transitions. NMR as well as electrochemical investigations and UV-Vis absorption suggest a polarization of the complexes with the negative charge pushed towards the 4*H*-imidazolate moiety.

Introduction

2-Aryl-5-arylamino-4-arylimino-4*H*-imidazoles (in the following referred to as 4*H*-imidazoles; *cf.* **HN1** and **HN2** in Figure 1) and some of their transition metal complexes, *e.g.* ruthenium complexes show broad and intense absorption features in the visible range of the electromagnetic spectrum. The absorption properties of the 4*H*-imidazoles as well as of their metal complexes are tuneable by the choice of the 2-aryl and *N*-aryl substituents as well as by the choice of the metal centre.[1–7] The panchromatic absorption in the visible range of these compounds suggests their application as photosensitizers *e.g.* for dye-sensitized solar cells or as sensitizers in photocatalysis.[8–10] The 2-aryl-5-arylamino-4-arylimino-4*H*-imidazoles (*cf.* **HN1** and **HN2** in Figure 1) are Wurster-type two-step redox systems with a cyclic π-system and exocyclic end groups, which can be reversibly reduced by two consecutive electron transfer steps.[11] But also the 4*H*-imidazole-derived ruthenium complexes are able to reversibly store two electrons,[3] this property renders these compounds interesting candidates for two electron photocatalysis such as CO_2 or proton reduction catalysis or for application in molecular electronics.[9] For instance, in the case of a previously published [Ru(II)(terpyridine)(**N1**)Cl] complex (*cf.* Figure 1) two electrons can be stored on the 4*H*-imidazolate ligand. When the *N*-aryl substituent of the 4*H*-imidazolate ligand was *p*-tolyl rather than 4-ethylcarboxyphenyl (CH_3 instead of COOEt in **N1**, *cf.* Figure 1) reduction lead to the first electron being localized on the 4*H*-imidazolate ligand and the second electron being localised on the terpyridine ligand.[12] These observations emphasize the possibility to not only control the redox potential but also the localisation of the excited state on particular parts of the complex by subtle structural modifications of 4*H*-imidazolate complexes. Very recently the charge injection efficiency of ruthenium 4*H*-imidazolates into TiO_2 was studied.[8] Besides their redox chemistry, 4*H*-imidazoles and their ruthenium complexes also show an interesting acid base chemistry. In typical 4*H*-imidazoles the neutral merocyanine type is red, the cationic cyanine type is blue to green and the anionic oxonole is violet.[3] Protonation of Ru(II)-4*H*-imidazolates red shifts the intense metal-to-ligand charge transfer (MLCT) absorption and leads to swapping of the relative energetic position of excited triplet states, which are involved in the deactivation of the complex after excitation by light.[13]

Besides the well investigated ruthenium complexes also Pd(II),[14] Ni(II),[14] Ir(III),[5] Zn(II) [2] an Cu(II) [2] complexes were examined. While copper(I) complexes of *e.g.* phenanthroline or bipyridine are in the focus of present research activities, [15–28] copper(I) complexes

[a] Institute for Physical Chemistry and Abbe Center of Photonics, Friedrich-Schiller University Jena, Helmholtzweg 4, 07743 Jena, Germany. E-mail: martin.schulz.1@uni-jena.de
[b] Leibniz Institute of Photonic Technology (IPHT) Jena e. V., Albert-Einstein-Str. 9, 07745 Jena, Germany.
[c] Institute for Inorganic and Analytical Chemistry, Friedrich-Schiller University Jena, Humboldtstr. 8, 07743 Jena, Germany.

† Electronic Supplementary Information (ESI) available: Crystallographic data (excluding structure factors) has been deposited with the Cambridge Crystallographic Data Centre as supplementary publication CCDC-1432665 for **CuN1P1**, CCDC-1432667 for **CuN2P1**, CCDC-1432666 for **CuN1P2**, and CCDC-1432668 for **CuN2P2**. Copies of the data can be obtained free of charge on application to CCDC, 12 Union Road, Cambridge CB2 1EZ, UK [E- mail: deposit@ccdc.cam.ac.uk]. Molecular structures and refinement data, UV-Vis absorption and emission data as well as percent contributions to selected frontier orbitals are given in the ESI. See DOI: 10.1039/x0xx00000x

of 4*H*-imidazoles are unknown as of yet. The present study lays the basis to exploit this novel class of copper(I)-complexes. Deprotonation of 4*H*-imidazoles affords a bidentate monoanionic 4*H*-imidazolate ligands, which are well suited for copper(I) complexation. The contribution at hand presents a facile synthetic access to novel heteroleptic copper(I)-4*H*-imidazolate complexes and investigates their structural, spectral and redox properties.

Results and discussion

Synthesis

The employed 4*H*-imidazole and bisphosphane ligands are depicted in Figure 1. The heteroleptic [Cu(I)(PP)(NN)] copper(I) complexes (**CuN1P1**, **CuN1P2**, **CuN2P1** and **CuN2P2**) were synthesized from $[Cu(acetonitrile)_4]^+ (PF_6)^-$ by sequential addition of the ligands starting with the bulky phosphanes. Addition of the neutral 4*H*-imidazole ligand to the copper phosphane complex solution in the presence of the weakly basic anion exchange resin Amberlyst A21 afforded a deep violet solution. The reaction mixture was stirred overnight monitoring the progress by UV-Vis absorption spectroscopy. Crystalline compounds were obtained by slow solvent evaporation of dichloromethane/*n*-hexane or acetone/*n*-hexane solutions yielding analytically pure compounds. The overall, non-optimised yields were between 40% and 70%. All complexes were characterised by ^{1}H- and ^{31}P-NMR spectroscopy, mass spectrometry, elemental analysis as well as single crystal X-ray diffraction. All synthesized complexes are stable in solution as well as solids under atmospheric conditions. However, they are sensitive towards acids and react under decomplexation and formation of the free 4*H*-imidazole (*vide infra*).

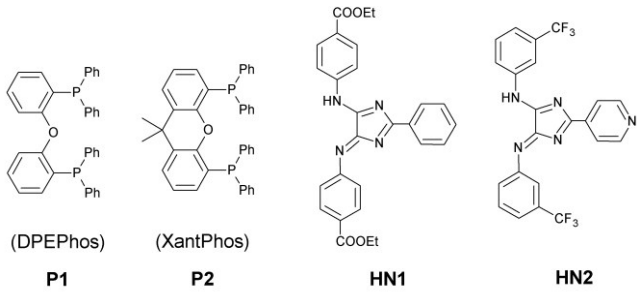

Figure 1 depicts the phosphane and 4*H*-imidazole ligands used in this study.

Characterization

^{1}H- and ^{31}P-NMR spectroscopy. The reported complexes were studied by ^{1}H- and ^{31}P-NMR spectroscopy (see ESI). A single ^{31}P-NMR signal was observed for each complex in the range between -12 to -14 ppm, which is within the expected range for heteroleptic [Cu(I)(NN)(PP)] complexes.[20] The ^{31}P-signal of the PF_6^- anion was absent in all cases. Comparison of the ^{31}P-NMR data of [**CuN1P1**] and [**CuN2P1**] with those of free **P1** as well as of those of the homoleptic $[Cu(I)(\mathbf{P1})_2]^+$ indicate the formation of the neutral heteroleptic complexes in solution. The same conclusions can be drawn for the complexes [**CuN1P2**] and [**CuN2P2**] based on the comparison of the ^{1}H-NMR data[29] of $[Cu(I)(\mathbf{P2})_2]^+$ with that of free **P2** as well as of the ^{1}H-NMR data of [**CuN1P2**] and [**CuN2P2**] (^{31}P-NMR data of $[Cu(I)(\mathbf{P2})_2]^+$ is not reported in the literature). The ^{1}H-NMR spectra of all complexes show a 1:1 ratio of the phosphane as well as the 4*H*-imidazolate integrals. Based on the above described observations and on steric considerations we conclude that the reported complexes adopt a mononuclear [Cu(I)(NN)(PP)] constitution in solution (and not $[Cu(I)_2(NN)_2(PP)_2]$) or $[Cu(I)(PP)_2]^+[Cu(I)(NN)_2]^-$).[30,31] This conclusion is supported by ESI mass spectrometry data and X-ray diffraction results (*vide infra*). Mass spectra were taken from an acetonitrile/methanol solution and comparison of the experimental and calculated isotope pattern confirms the formation of the mononuclear heteroleptic complexes. The most intensive signal could be assigned to $[M+H]^+$ for **[CuN1P1]** and [**CuN1P2**] as well as $[M+Na]^+$ for the 4-pyridyl containing [**CuN2P1**] and [**CuN2P2**]. Furthermore, $[M-\mathbf{N1}]^+$ and $[M-\mathbf{N2}]^+$ signals were observed.

Complexation of the 4*H*-imidazolate by the copper(I)-phosphane fragment induced a considerable highfield shift of all 4*H*-imidazolate protons in the ^{1}H-NMR spectrum. With respect to the uncoordinated neutral 4*H*-imidazole, the highfield shift is about 0.1 ppm for the 2-aryl ring and of about 0.5 – 0.6 ppm for both *N*-aryl rings. As a comparison, deprotonation of free 4*H*-imidazole by triethylamine (15-fold molar excess) induces a slight highfield shift of about 0.01 - 0.03 ppm for all aryl protons. In contrast, lowfield shifting of most phosphane signals is observed for all complexes in the ^{1}H-NMR spectrum. The negative charge is delocalized over the 4*H*-imidazolate ligand and the extent of which is governed by the aryl-bound substituents of the 4*H*-imidazolate ligand. This is also supported by electrochemical data (*vide infra*), which shows a shift towards more negative potentials of the 4*H*-imidazolate-based reduction waves of the complexes with respect to the free 4*H*-imidazolate. Furthermore, two effects lead to the observed highfield shift of the 4*H*-imidazolates and the lowfield shift of the phosphanes, namely charge-induced shielding of the 4*H*-imidazolate protons and ring current effects due the close proximity of the 4*H*-imidazolate *N*-aryl rings and the phosphane aryls (*cf.* Crystallography section). However, the charge induced shielding in the free 4*H*-imidazolates is less pronounced than in the complexes. This observation may be interpreted as a complexation induced polarization of the ligands.

Crystallography. All synthesized compounds could be crystallized either from a mixture of acetone/*n*-hexane or dichloromethane/*n*-hexane. The complexes **CuN1P1**, **CuN2P1** and **CuN1P2** crystallized in the triclinic space group $P\bar{1}$ while **CuN2P2** crystallized in the monoclinic space group $P2_1/c$. All complexes were found to be of the mononuclear [Cu(I)(NN)(PP)] type and the molecular structure of **CuN1P2**

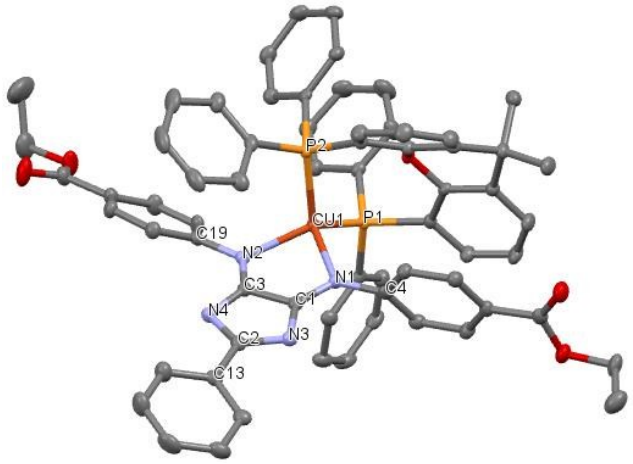

Figure 2 gives the molecular structure of **CuN1P2** with ellipsoids drawn at the 50% probability level. Hydrogen atoms and solvent molecules are omitted for clarity.

is exemplarily depicted in Figure 2 (see ESI, Figures S12-S14 for more structures).

All complexes show heavily distorted tetrahedral copper coordination with N1-Cu-N2 angles of about 82° and P1-Cu-P2 angles of 113-117° (see Table 1). Expectedly, the N-Cu-N angles are slightly larger than those reported for copper(I)-diimine complexes such as phenanthroline or bipyridine.[31,32] **CuN2P2** shows a slightly larger P-Cu-P angle which is attributed to packing effects. The planes spanned by P1-Cu-P2 and N1-Cu-N2 are not perpendicular but twisted to 87.33° (**CuN1P1**), 84.83° (**CuN2P1**), 81.30° (**CuN1P2**), 82.46° (**CuN2P2**). This twist depends on the phosphane ligand and is larger for the more rigid phosphane **P2**.

All bond lengths are in the expected range and are summarized in Table 1. The imidazole ring C-N bond lengths are between single and double bond while the C1-C3 bond is about 1.5 Å in all complexes (see Table 1). The 2-aryl rings are not coplanar with the imidazole ring plane and adopt dihedral angles of 16.41° (**CuN1P1**), 20.64° (**CuN1P2**), 24.16° (**CuN2P1**), 11.24° (**CuN2P2**). The *N*-aryl rings mostly show larger dihedral angles between the *N*-aryl and the Cu-N1-C1-C3-N2 plane. X-ray diffraction data suggests that all rings can rotate freely. This is supported by ^{1}H-NMR data. Although in **CuN1P2** one *N*-aryl ring is nearly coplanar with one phenyl ring of the **P2** xanthene moiety, with the closest distance of about 3.8 Å. A similar π-π interaction was observed in **CuN1P2** for two nearly coplanar, *P*-bound phenyl rings with the closest distance of about 3.5 Å as well as in **CuN2P1** between a *P*-bound phenyl ring and a phenylether ring (closest distance of about 3.4 Å). Despite the small distance, the complexes **CuN1P1** and **CuN2P2** do not show this type of π-π interactions, although possible. The interactions are therefore considered to be weak.

Table 1 gives selected bond lengths (Å) and angles (°).

Parameter	CuN1P1	CuN1P2	CuN2P1	CuN2P2
Cu-P1	2.2660(6)	2.2242(8)	2.3006(9)	2.2433(6)
Cu-P2	2.2806(6)	2.2653(8)	2.2472(8)	2.2809(6)
Cu-N1	2.1029(17)	2.093(2)	2.125(2)	2.0981(19)
Cu-N2	2.1470(17)	2.073(2)	2.099(3)	2.1096(19)
C1-C3	1.495(3)	1.502(4)	1.495(4)	1.500(3)
C1-N1	1.309(3)	1.297(4)	1.306(4)	1.300(3)
C3-N2	1.312(3)	1.307(4)	1.299(4)	1.312(3)
N1-C4	1.413(3)	1.421(4)	1.422(4)	1.420(3)
N2-C19	1.412(3)	1.413(4)	1.421(4)	1.413(3)
C2-C13	1.471(3)	1.477(4)	1.480(4)	1.473(3)
N1-Cu-N2	82.10(6)	82.24(9)	82.32(10)	82.31(7)
P1-Cu-P2	114.56(2)	113.90(3)	113.85(3)	116.96(2)

Electrochemistry. The ground state redox properties of the all reported complexes were investigated by cyclic voltammetry as well as square wave voltammetry at a Pt-electrode in dichloromethane against Ag/AgCl reference electrode. Ferrocene was added at the end of the experiment and all presented electrochemical potentials are referenced against the Fc/Fc^{+} couple ($E_{1/2}(Fc/Fc^{+})$ = 0.560 V). The results are summarized in Table 2 and in the Figures S6-S7 in the ESI. Both the cathodic and anodic processes are electrochemically irreversible.

Within the experimental window all compounds show one anodic wave, which is assigned to a copper based oxidation process. The assignment is based on the comparison with the oxidation potential of [Cu(phenanthroline)**P1**]$^{+}$ (0.75 V *vs.* Fc/Fc^{+}) and [Cu(2,9-(dimethyl)phenanthroline)**P1**]$^{+}$ (0.88 V *vs.* Fc/Fc^{+}).[31] For the **P1** containing compounds the flank of a second anodic process at potentials larger than 1.5 V was observable, which could possibly be due to phosphane based oxidations.[30,33] Observation of the complete second anodic wave of **P1** containing compounds was outside the electrochemical window for dichloromethane. Also, for the **P2** containing compounds no second oxidation wave at all could be observed under the experimental conditions. The oxidation potentials are influenced both by the phosphane as well as by the 4*H*-imidazolate ligand, while the latter is having a more pronounced effect on the position of the oxidation peaks. A general trend towards more positive values is observed when going from **P1** to **P2** (ca. 40 mV) and from **N1** to **N2** (ca. 130 mV).

In the cathodic region two distinct waves were observed, which are both assigned to the reduction of the 4*H*-imidazolate ligand. The reduction of free **N1**$^{-1}$ occurs at: $E_{red,1}$ = 1.51 V; $E_{red,2}$ = 1.72 V (*vs.* Fc/Fc^{+}). Comparison of the first reduction potential in dependence on the 4*H*-imidazolate ligand reveals that, the **N1** containing compounds show more negative values (ca. 30 mV) than the **N2** containing compounds. The opposite behaviour is observed for the second reduction wave (ca. 70-100 mV). Also a slight effect of the phosphane ligands on the first 4*H*-imidazolate reduction was observed showing a trend towards more negative values when going from **P2** to **P1** (ca. 20 mV). The opposite effect

was observed for the second reduction process for the **N2** containing compounds, *i.e.* a trend towards more negative potentials when going from **P1** to **P2** (40 mV). The phosphane-induced potential difference for the **N1** containing compounds is negligible. At this stage, the irreversible nature of the electrochemical processes precludes any further discussions.

Table 2 gives the electrochemical properties of the reported complexes.

Compound	E_{red}[a] in V	E_{ox}[a] in V
CuN1P1	–1.71, –2.07	+0.59
CuN2P1	–1.68, –2.14	+0.72
CuN1P2	–1.69, –2.08	+0.63
CuN2P2	–1.66, –2.18	+0.76

[a] Square wave voltammetry in dichloromethane with 0.1 M tetra-butylammonium BF_4^- *vs.* Fc/Fc^+ couple with a step potential of 5 mV and a frequency of 64 Hz.

UV-Vis spectroscopy. The UV-Vis spectra of the reported complexes are given in Figure 3 and are governed by two major bands, one smaller band in the UV region with the maximum between 250-300 nm and a broad less intense band ranging from about 400 to 600 nm with maxima between 517-530 nm (see Figure 3). The shape of the bands is mainly governed by the 4*H*-imidazolate ligands. Comparison of the UV-Vis data of the parent 4*H*-imidazole with the free, deprotonated 4*H*-imidazolate and the respective complexes reveals a deprotonation-induced red shift and significant broadening upon complexation with the copper phosphane fragment at the high energy site of the low energy absorption band. This suggests contributions of copper based orbitals to the transitions in the visible region while the UV region is governed by inner ligand and ligand to ligand charge transfer transitions. These suggestions are supported by TD-DFT calculations on **CuN2P2** (*vide infra*).

All complexes exhibit very weak emission, which was only detectable with a sensitive, cooled CCD detector upon laser excitation at 532 nm (see Figure S11, ESI). Noteworthy, all emission spectra show three distinguishable bands. Experiments to elucidate the origin of the emission as well as excited state lifetime studies are underway.

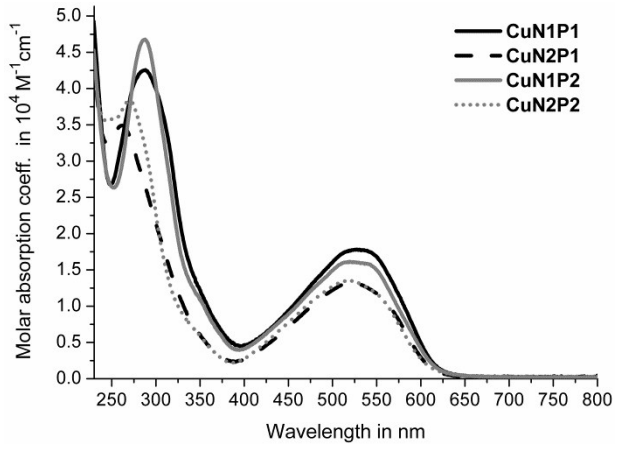

Figure 3 depicts the UV-Vis absorption spectra of the reported complexes. Spectra were taken in acetonitrile. The molar absorption coefficients were determined with four different concentrations.

Protonation can have a substantial impact on the absorption properties of 4*H*-imidazolate complexes. An earlier reported [Ru(II)(4*H*-imidazolate)(terpyridine)Cl] complex shows a red-shift of the low energy MLCT absorption band upon protonation together with considerable differences in the Franck-Condon points between the protonated and unprotonated species.[13] In a combined theoretical and experimental study it was found that charge transfer transitions to the imidazole sphere are favoured for the protonated [Ru(II)(4*H*-imidazole)(terpyridine)Cl]$^+$. This is an important aspect, if directed charge-transfer is desired.

Protonation of the copper(I) complexes presented in this contribution was followed by a colour change from violet to yellow. This was first discovered on silica TLC-sheets during attempts to monitor the reaction. In order to unravel the acid-dependent colour change, UV-Vis titration studies using trifluoroacetic acid (TFA) in acetonitrile were conducted. The spectral changes over the course of the TFA titration of **CuN1P1** are given in Figure 4 (see ESI for further details). Upon addition of TFA a decrease of the low-energy flank of the Vis absorption band as well as around 300 nm is observed together with an overall increase of absorption in the range between 328–497 nm. These changes are indicative for the formation of the neutral 4*H*-imidazole. The inset in Figure 4 gives a comparison between the normalized UV-Vis absorption spectra of the titration endpoint and that of free neutral 4*H*-imidazole indicating the complete decomposition of the complex into 4*H*-imidazole and a copper(I) species, probably [Cu(I)(phosphane)(aceto-

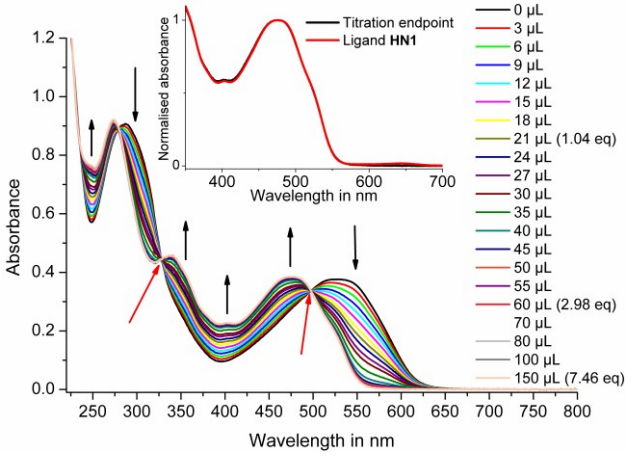

Figure 4 presents the spectral change of solution of **CuN1P1** over the course of titration with trifluoroacetic acid in acetonitrile. The total volume of TFA in the solution is given together with the molar equivalents, with respect to the complex, in parentheses. Isosbestic points are marked with red arrows (328 nm; 497 nm). The inset compares the UV-Vis spectrum of the titration endpoint (black) with the UV-Vis spectrum of the neutral 4*H*-imidazole ligand **HN1** in acetonitrile (red), normalised to the absorption maximum.

nitrile)$_2$]$^+$, which does not absorb in the visible region. These results show that the colour change is associated with dissociation of the 4*H*-imidazolate ligand and its protonation under formation of the neutral 4*H*-imidazole. No intermediate species, such as a protonated Cu(I)-4*H*-imidazole complex as in the case of the Ru(II)-complexes could be observed.

Addition of an excess of the strong base 1,7-diazabicylco-undec-7-ene (DBU) led to a partial recovery of the spectral signatures of the copper(I)-4*H*-imidazolate complexes (see ESI for further details). In fact, the obtained spectra can be regarded as a mixture of the spectra of free anionic 4*H*-imidazolate and the respective Cu(I)-4*H*-imidazolate complex. The degree of recovery correlates with synthetic yield of the complexes showing higher values for the **P2** containing compounds.

TD-DFT calculations. Time-dependent DFT calculations (TD-DFT) were used in order to investigate the nature of the observed electronic transitions in the visible spectrum of **CuN2P2**. Vertical excitations were calculated using the CAM-B3LYP functional[34] based on the geometry optimized ground state structure. Although CAM-B3LYP often overestimates the energy of metal-to-ligand charge transfer transitions the band shape is usually well described. TD-DFT results show two major transitions at 466 nm and 418 nm and two minor transitions at 392 nm and 369 nm that compose the band in the visible spectrum. The calculated band shape agrees very well with the experimental but appears blue-shifted by about 65 nm. The four transitions, which compose the band in the visible spectrum, have charge transfer character. The major contributions are given in Table 3 (*cf.* Table S2, and Figure S15 ESI).

Table 3 gives the wavelengths (nm) energy (eV), oscillator strengths *f* and major contributions to the first four singlet transitions for **CuN2P2** based on TD-CAM-B3LYP calculations.

Trans.	λ in nm	E in eV	*f*	Major contributions
S_1	466	2.66	0.2534	H-1->LUMO (42%), HOMO->LUMO (49%)
S_2	418	2.97	0.2032	H-1->LUMO (44%), HOMO->LUMO (36%)
S_3	392	3.16	0.0188	H-3->LUMO (74%)
S_4	369	3.36	0.0069	H-2->LUMO (70%)

Table 3 shows that the LUMO is the only acceptor orbital while the H-3, H-2, H-1 and the HOMO constitute the major donor orbitals. A Mullikan population analysis using the M06 functional reveals a 4*H*-imidazolate based LUMO with negligible contributions of copper (2%) and phosphane (2%). Within the 4*H*-imidazolate ligand the imidazolate moiety (60%) as well as *N*-aryl rings (17%) and the 2-aryl ring (20%) contribute to this orbital. The four donor orbitals (HOMO, H-1, H-2 and H-3) are mixed with significant contributions of copper and the imidazolate moiety as well as with significant contributions of the *N*-aryl rings to H-1 and H-3 and the phosphane ligand to HOMO and H-2. The 2-aryl ring has negligible contributions to all four orbitals (*cf.* Figure 5, and Table S2, ESI).

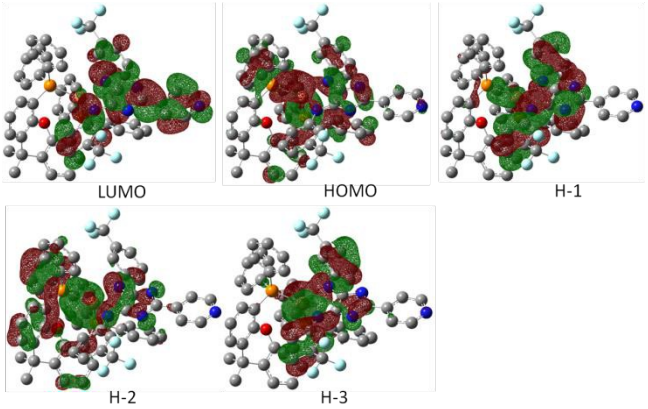

Figure 5 depicts the frontier orbitals of **CuP2N2** (M06). These orbitals are the major donor and acceptor orbitals for the low energy electronic transitions.

Conclusion

Four neutral, heteroleptic copper(I)-4*H*-imidazolate complexes with either a XantPhos or DPEPhos ligand were synthesized and structurally characterized by ^{1}H and ^{31}P NMR spectroscopy, mass spectrometry, elemental analysis as well as single crystal X-ray diffraction. The obtained data confirms the formation of the neutral, mononuclear, heteroleptic [Cu(I)(PP)(NN)] complexes in the solid state as well as in solution. NMR investigations as well as electrochemistry data show a polarization of the complexes with negative charge pushed towards the 4*H*-imidazolate moiety, with respect to the free ligands. All four complexes exhibit a broad absorption band in the visible range of the spectrum with extinction coefficients around 1.5×10^4 $M^{-1}cm^{-1}$. TD-DFT calculations revealed that the involved transitions have charge transfer character, *i.e.* from the phosphane-copper sphere to the 4*H*-imidazolate sphere. These properties render these complexes potential candidates as photosensitizers for *e.g.* dye-sensitised solar cells or photocatalysis. Despite the sensitivity of the complexes towards acids they are stable in neutral and basic solutions as well as solids under atmospheric conditions. Importantly, the acid induced decomplexation is reversible within the limits of the complexation equilibria.

The spectral properties of the 4*H*-imidazoles as well as their electrochemical properties are tuneable by selection of the 2-aryl and *N*-aryl bound substituents.[2–4,35,36] Novel copper complexes with tuneable properties might be expected by virtue of the access to a wide variety of 4*H*-imidazoles, reported by Beckert and coworkers and the facile access to this new class of copper complexes, gained in this work.

Experimental

Instrumentation. ^{1}H- and ^{31}P{1H}-NMR spectra were recorded on a Bruker Advance AC400 spectrometer with a resonance frequency of 400 MHz and 162 MHz respectively at 25°C. The signal was locked to the solvent residual peak. ESI-MS mass spectra were recorded either on a Finnigan MAZ95XL or on a Finnigan MAT SSQ 710. UV-Vis spectra were recorded either on a Varian Cary 5000 UV-Vis-NIR spectrometer or on a Perkin-Elmer Lambda 16 UV-Vis spectrometer using quartz cuvettes with an optical path length of 1 cm and acetonitrile as solvent. Emission spectra were recorded with a cooled PIXIS 400-eXcelon CCD attached to an Isoplane 320 spectrograph obtained from Princeton Instruments. The setup is optimized for measuring red and NIR emission. A frequency-doubled Nd-YAG-laser with a wavelength of 532 nm and 5 mW (cw) was used as excitation source. Electrochemical data was collected on an EcoChemie Autolab PGSTAT20 with a platinum disc as working electrode, glassy carbon as a counter electrode and Ag/AgCl as reference electrode at 20°C. Ferrocene was added at the end of the experiment and all presented electrochemical potentials are referenced against the Fc/Fc^{+} couple ($E_{1/2}(Fc/Fc^{+})$ = 0.560 V *vs*. Ag/AgCl). Dichloromethane was dried over P_2O_5 and distilled under argon atmosphere. The sample concentration was about $5 \cdot 10^{-4}$ M in anhydrous dichloromethane and 0.1 M tetrabutylammonium tetrafluoroborate was used as electrolyte. The electrochemical cell was purged with nitrogen prior to and between the experiments.

General synthetic procedure. All manipulations were carried out under argon atmosphere using standard Schlenk techniques. The copper(I) precursor as well as the phosphanes were commercially obtained and used as received. The synthesis of the 4*H*-imidazole ligands is described elsewhere.[1]

In a 100 mL round bottom flask the phosphane (0.18 mmol, 1 eq.) was dissolved in 50 mL of dichloromethane. The colourless solution was then transferred to a 100 mL Schlenk flask containing $[Cu(acetonitrile)_4]PF_6$ (0.18 mmol, 1.0 eq.) and the mixture was stirred for 1.5 h until all solid particles were dissolved. Then two spatula tips (approx. 10 mg) of dry Amberlyst A21 were added and the resulting dispersion was stirred for 0.5 h. Subsequently, a solution of 4*H*-imidazole (0.18 mmol, 1.0 eq.) in 8 mL of dichloromethane were added dropwise into the reaction flask over a period of 20 min. Instantly, the colour of the reaction mixture changed to reddish violet and the reaction mixture was allowed to stir for additional 16 hours. After that time, the Amberlyst A21 beads were removed from the mixture by filtration and the solvent was removed *in vacuo*. The obtained dark red precipitate was then dissolved in a mixture of *n*-hexane and acetone 5:1 (v/v). Unreacted 4*H*-imidazole ligand was removed by separation on a basic aluminium oxide (Brockmann I) column. The violet fraction was collected and the products were obtained by evaporation of the solvents. Crystallization was achieved by slow solvent evaporation from either *n*-hexane/acetone or *n*-hexane/dichloromethane solutions.

CuN1P1. Yield: 80 mg (40 %) of dark red crystalline solid. ^{1}H-NMR (400 MHz, dichloromethane-d_2) ppm: 1.38 (t, J = 7.02 Hz, 6H), 4.33 (q, J = 7.12 Hz, 4H), 6.71–6.77(m, 2H), 6.84–6.97 (m, 4H), 7.05–7.30 (m, 22H), 7.33–7.40 (m, 4H), 7.41–7.49 (m, 2H), 7.50–7.58 (m, 1H), 7.61–7.70 (m, 4H), 8.32–8.42 (m, 2H). ^{31}P{^{1}H}-NMR (162 MHz, dichloromethane-d_2) ppm: -13.67. MS (Micro-ESI pos. in dichloromethane/methanol) m/z: 1091 $[M+Na^{+}]^{+}$, 1069 $[M+H^{+}]^{+}$, 601 $[(M\text{-}\mathbf{N1})]^{+}$. CHN analysis: $C_{63}H_{51}CuN_4O_5P_2$ (1069.60 $gmol^{-1}$), calcd. C 70.74%, H 4.81%, N 5.24%; found C 69.12%, H 4.61%, N 5.12% (The low carbon content is attributed to carbide formation during elemental analysis).

CuN1P2. Yield: 130 mg (65 %) of a dark red crystalline solid. 1H-NMR (400 MHz, dichloromethane-d_2) ppm: 1.39 (t, J = 7.17 Hz, 6 H), 1.66 (s, 6H), 4.32 (q, J = 7.02 Hz, 4H), 6.44–6.56 (m, 2H), 7.00–7.18 (m, 22H), 7.26 (t, J = 7.02 Hz, 4H), 7:40–7:62 (m, 9H), 8.34–8.46 (m, 2H). ^{31}P{^{1}H}NMR (162 MHz, dichloromethane-d_2) ppm: -13.03. MS (Micro-ESI pos. in dichloromethane/methanol) m/z: 2219, 1751, 1164, 1110 $[M+H^{+}]^{+}$, 642 $[(M\text{-}\mathbf{N1})]^{+}$. CHN analysis: $C_{66}H_{55}CuN_4O_5P_2$ (1109.66 $gmol^{-1}$), calcd. C 71.44%, H 5.00%, N 5.05%; found C 71.05%, H 5.23%, N 4.55%.

CuN2P1. Yield: 90 mg (45 %) of a dark red crystalline solid. 1H-NMR (400 MHz, acetonitrile-d_3) ppm: 6.71–6.79 (m, 2H), 6.88–6.93 (m, 2H), 6.96 (td, J = 7.55; 1.07 Hz, 2H), 7.04–7:35 (m, 26H), 7.50 (d, J = 7.93 Hz, 2H), 7.64 (s, 2H), 8.06 (d, J = 5.80 Hz, 2H), 8.71 (d, J = 5.49 Hz, 2H). ^{31}P{^{1}H}-NMR (162 MHz, acetonitrile-d_3) ppm: -13.42. MS (Micro-ESI pos. in dichloromethane/ methanol) m/z: 1602, 1085 $[M+Na^{+}]^{+}$, 602 $[M\text{-}\mathbf{N2}]^{+}$. CHN analysis: $C_{58}H_{40}CuF_6N_5OP_2$ (1062.45 $gmol^{-1}$), calcd. C 65.57%, H 3.79%, N 6.59%; found C 65.72%, H 3.74%, N 6.58%.

CuN2P2. Yield: 141 mg (70.5 %) of dark red crystalline solid. ^{1}H-NMR (400 MHz, chloroform-d_1) ppm: 1.66 (s, 6H), 6.49–6.59 (m, 2H), 6.78–6.94 (m, 4H), 6.97–7.20 (m, 20H), 7.25 (t, J = 6.70 Hz, 4H), 7.49 (dd, J = 7.78, 1.37 Hz, 2H), 7.72 (s, 2H), 8.22 (d, J = 5.80 Hz, 2H), 8.75 (d, J = 5.19 Hz, 2H). ^{31}P{^{1}H} NMR (162 MHz, chloroform-d_1) ppm: -12.58. ESI-MS (Micro-ESI pos. in dichloromethane/methanol) m/z: 2227, 1744, 1157, 1125 $[M+Na^{+}]^{+}$, 642 $[M\text{-}\mathbf{N2}]^{+}$. CHN analysis: $C_{61}H_{44}CuF_6N_5OP_2$ (1102.52 $gmol^{-1}$), calcd. C 66.45%, H 4.02%, N 6.35%; found C 66.57%, H 3.81%, N 6.31%.

Structure determination. The intensity data for the compounds were collected on a Nonius KappaCCD diffractometer using graphite-monochromated Mo-Kα radiation. Data were corrected for Lorentz and polarization effects; absorption was taken into account on a semi-empirical basis using multiple-scans.[37–39] The structures were solved by direct methods (SHELXS[40]) and refined by full-matrix least squares techniques against Fo^2 (SHELXL-97[41]). The hydrogen atoms of **CuN1P1** (with exception of disordered ethyl group) and **CuN2P2** were located by difference Fourier synthesis and refined isotropically. All other hydrogen atoms were included at calculated positions with fixed thermal parameters. All non-disordered, non-hydrogen atoms were refined anisotropically.[41] The crystal of **CuN2P1** contains large voids, filled with disordered solvent molecules. The size of the voids is 406 $Å^3$/unit cell. Their contribution to the structure factors was secured by back-Fourier transformation using the SQUEEZE routine of

the program PLATON[42] resulting in 83 electrons/unit cell. Crystallographic data as well as structure solution and refinement details are summarized in Table S1, ESI. XP (SIEMENS Analytical X-ray Instruments, Inc.) was used for structure representations.

Computational method. All calculations were carried out with the Gaussian 09 program suite.[43] The geometries were optimized using the M06 functional.[44] The MDF10 basis[45] with an effective core potential was used for the Cu atom while 6-31G(d)[46] was used for the remainder. Tight convergence criteria were applied for the geometry optimization process and local minima were confirmed by a frequency calculation. Geometry optimizations were carried out in the presence of a solvent sphere, which was modelled by the IEF-PCM[47] method in dichloromethane (ε=8.93). Orbital contributions were calculated by a Mulliken population analysis and evaluated using GaussSum.[48] Vertical excitations were modelled by a TD-DFT calculation with the geometry optimized ground state structures using the CAM-B3LYP[34] functional and the MDF10 and 6-31G(d) basis set as explained above. The solvent sphere was modelled using IEF-PCM formalism with dichloromethane (ε=8.93) and acetonitrile (ε=35.688).

Acknowledgements

Prof. Rainer Beckert, University Jena, is gratefully acknowledged for the allocation of the 4*H*-imidazole ligands. Sven Krieck, University Jena, is thanked for assistance with the electrochemistry experiments.

Notes and references

1 J. Atzrodt, J. Brandenburg, C. Käpplinger, R. Beckert, W. Günther, H. Görls and J. Fabian, *J. für Prakt. Chemie Chem.*, 1997, **339**, 729–734.
2 R. Beckert, C. Hippius, T. Gebauer, F. Stöckner, C. Lüdigk, D. Weiß, D. Raabe, W. Günther and H. Görls, *Z. Naturforsch., B Chem. Sci.*, 2006, **61**, 437–447.
3 M. Matschke and R. Beckert, *Molecules*, 2007, **12**, 723–734.
4 M. Matschke, J. Blumhoff, R. Beckert and W. Imhof, *Z. Naturforsch., B Chem. Sci.*, 2009, **64**, 624–628.
5 J. Blumhoff, R. Beckert, S. Rau, S. Losse, M. Matschke, W. Günther and H. Görls, *Eur. J. Inorg. Chem.*, 2009, **2009**, 2162–2169.
6 M. Wächtler, S. Kupfer, J. Guthmuller, S. Rau, L. González and B. Dietzek, *J. Phys. Chem. C*, 2012, **116**, 25664–25676.
7 M. Wächtler, M. Maiuri, D. Brida, J. Popp, S. Rau, G. Cerullo and B. Dietzek, *ChemPhysChem*, 2013, 1–12.
8 J. Schindler, S. Kupfer, M. Wächtler, J. Guthmuller, S. Rau and B. Dietzek, *ChemPhysChem*, 2015, **16**, 1061–70.
9 M. Schulz, M. Karnahl, M. Schwalbe and J. G. Vos, *Coord. Chem. Rev.*, 2012, **256**, 1682–1705.
10 Y. Zhang, S. Kupfer, L. Zedler, J. Schindler, T. Bocklitz, J. Guthmuller, S. Rau and B. Dietzek, *Phys. Chem. Chem. Phys.*, 2015, 20–27.
11 K. Deuchert and S. Hünig, *Angew. Chem.*, 1978, **90**, 927–938.
12 L. Zedler, S. Kupfer, I. R. de Moraes, M. Wächtler, R. Beckert, M. Schmitt, J. Popp, S. Rau and B. Dietzek, *Chem. Eur. J.*, 2014, **20**, 3793–9.
13 S. Kupfer, J. Guthmuller, M. Wächtler, S. Losse, S. Rau, B. Dietzek, J. Popp and L. González, *Phys. Chem. Chem. Phys.*, 2011, **13**, 15580–8.
14 J. Blumhoff, R. Beckert, D. Walther, S. Rau, M. Rudolph, H. Görls and W. Plass, *Eur. J. Inorg. Chem.*, 2007, **2007**, 481–486.
15 N. Armaroli, *Chem. Soc. Rev.*, 2001, **30**, 113–124.
16 M. S. Lazorski and F. N. Castellano, *Polyhedron*, 2014, **82**, 57–70.
17 R. S. Khnayzer, C. E. McCusker, B. S. Olaiya and F. N. Castellano, *J. Am. Chem. Soc.*, 2013, **135**, 14068–70.
18 S. Tschierlei, M. Karnahl, N. Rockstroh, H. Junge, M. Beller and S. Lochbrunner, *ChemPhysChem*, 2014, 1–5.
19 M. Karnahl, E. Mejía, N. Rockstroh, S. Tschierlei, S.-P. Luo, K. Grabow, A. Kruth, V. Brüser, H. Junge, S. Lochbrunner and M. Beller, *ChemCatChem*, 2014, **6**, 82–86.
20 S.-P. Luo, E. Mejía, A. Friedrich, A. Pazidis, H. Junge, A.-E. Surkus, R. Jackstell, S. Denurra, S. Gladiali, S. Lochbrunner and M. Beller, *Angew. Chem. Int. Ed*, 2013, **52**, 419–23.
21 Y.-J. Yuan, Z.-T. Yu, J.-Y. Zhang and Z.-G. Zou, *Dalton Trans.*, 2012, **41**, 9594–7.
22 X. Lu, S. Wei, C.-M. L. Wu, S. Li and W. Guo, *J. Phys. Chem. C*, 2011, **115**, 3753–3761.
23 C. L. Linfoot, P. Richardson, T. E. Hewat, O. Moudam, M. M. Forde, A. Collins, F. White and N. Robertson, *Dalton Trans.*, 2010, **39**, 8945–56.
24 E. C. Constable, A. Hernandez Redondo, C. E. Housecroft, M. Neuburger and S. Schaffner, *Dalton Trans.*, 2009, 6634–44.
25 N. Robertson, *ChemSusChem*, 2008, **1**, 977–9.
26 Y. Wang, F. Teng, Z. Xu, L. Qian, T. Zhang and D. Liu, *Prog. Nat. Sci.*, 2004, **14**, 746–752.
27 S. Sakaki, T. Kuroki and T. Hamada, *J. Chem. Soc. Dalton Trans.*, 2002, 840–842.
28 N. Alonso-Vante, J.-F. Nierengarten and J.-P. Sauvage, *J. Chem. Soc. Dalton Trans.*, 1994, **11**, 1649.
29 S. Medina-Rodríguez, F. J. Orriach-Fernández, C. Poole, P. Kumar, Á. de la Torre-Vega, J. F. Fernández-Sánchez, E. Baranoff and A. Fernández-Gutiérrez, *Chem. Commun.*, 2015, **51**, 11401–11404.
30 C. Femoni, S. Muzzioli, A. Palazzi, S. Stagni, S. Zacchini, F. Monti, G. Accorsi, M. Bolognesi, N. Armaroli, M. Massi, G. Valenti and M. Marcaccio, *Dalton Trans.*, 2013, 997–1010.
31 S.-M. Kuang, D. G. Cuttell, D. R. McMillin, P. E. Fanwick and R. A. Walton, *Inorg. Chem.*, 2002, **41**, 3313–3322.
32 M. T. Miller, P. K. Gantzel and T. B. Karpishin, *Inorg. Chem.*, 1999, **38**, 3414–3422.
33 A. Kaeser, O. Moudam, G. Accorsi, I. Séguy, J. Navarro, A. Belbakra, C. Duhayon, N. Armaroli, B. Delavaux-Nicot and J. F. Nierengarten, *Eur. J. Inorg. Chem.*, 2014, 1345–1355.
34 T. Yanai, D. P. Tew and N. C. Handy, *Chem. Phys. Lett.*, 2004, **393**, 51–57.
35 M. Matschke, R. Beckert, L. Kubicova and C. Biskup, *Synthesis*, 2008, 2957–2962.

36 M. Matschke, K. Knop and R. Beckert, *Struct. Chem.*, 2008, **19**, 399–405.
37 *COLLECT, Data Collection Software, Nonius B.V., Netherlands*, 1998.
38 Z. Otwinowski and W. Minor, in *Methods in Enzymology, Vol. 276, Macromolecular Crystallography, Part A*, eds. C. W. Carter and R. M. Sweet, Academic Press, 1997, pp. 307–326.
39 *SADABS 2.10, Bruker-AXS Inc., Madison, WI, U.S.A*, 2002.
40 G. M. Sheldrick, *Acta Crystallogr. Sect. A*, 2008, **64**, 112–122.
41 G. M. Sheldrick, *Acta Crystallogr. Sect. A*, 2008, **64**, 112–122.
42 A. L. Spek, *Acta Crystallogr. Sect. D*, 2009, **65**, 148–155.
43 M. J. Frisch, G. W. Trucks, H. B. Schlegel, G. E. Scuseria, M. A. Robb, J. R. Cheeseman, G. Scalmani, V. Barone, B. Mennucci, G. A. Petersson, H. Nakatsuji, M. Caricato, X. Li, H. P. Hratchian, A. F. Izmaylov, J. Bloino, G. Zheng, J. L. Sonnenberg, M. Hada, M. Ehara, K. Toyota, R. Fukuda, J. Hasegawa, M. Ishida, T. Nakajima, Y. Honda, O. Kitao, H. Nakai, T. Vreven, J. J. A. Montgomery, J. E. Peralta, F. Ogliaro, M. Bearpark, J. J. Heyd, E. Brothers, K. N. Kudin, V. N. Staroverov, R. Kobayashi, J. Normand, K. Raghavachari, A. Rendell, J. C. Burant, S. S. Iyengar, J. Tomasi, M. Cossi, N. Rega, J. M. Millam, M. Klene, J. E. Knox, J. B. Cross, V. Bakken, C. Adamo, J. Jaramillo, R. Gomperts, R. E. Stratmann, O. Yazyev, A. J. Austin, R. Cammi, C. Pomelli, J. W. Ochterski, R. L. Martin, K. Morokuma, V. G. Zakrzewski, G. A. Voth, P. Salvador, J. J. Dannenberg, S. Dapprich, A. D. Daniels, O. Farkas, J. B. Foresman, J. V Ortiz, J. Cioslowski and D. J. Fox, 2009.
44 Y. Zhao and D. G. Truhlar, *Theor. Chem. Acc.*, 2008, **120**, 215–241.
45 M. Dolg, U. Wedig, H. Stoll and H. Preuss, *J. Chem. Phys.*, 1987, **86**, 866.
46 V. A. Rassolov, J. A. Pople, M. A. Ratner and T. L. Windus, *J. Chem. Phys.*, 1998, **109**, 1223–1229.
47 J. Tomasi, B. Mennucci and R. Cammi, *Chem. Rev.*, 2005, **105**, 2999–3094.
48 N. M. O'Boyle, A. L. Tenderholt and K. M. Langner, *J. Comput. Chem.*, 2008, **29**, 839–845.